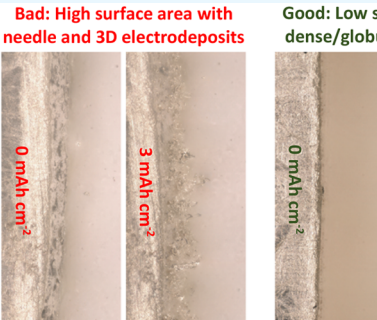
www.acsaem.org

Effect of the Electrolyte on the Cycling Efficiency of Lithium-Limited Cells and their Morphology Studied Through in Situ Optical Imaging

Rodrigo Rodriguez,[†] Kathryn E. Loeffler,[†] Ruth A. Edison,[†] Ryan M. Stephens,[⊥] Andrei Dolocan,[‡] Adam Heller,^{†,||} and C. Buddie Mullins**,^{†,‡,§,||}

Supporting Information

ABSTRACT: Capacity retention of anode-free cells, in which the cathode's lithium was the sole lithium source, was studied. These cells fail by depletion of their limited amount of cycling lithium, unlike cells with lithium foil anodes in which the buildup of an insulating, dead lithium layer on the anodes causes failure. The electrolyte dependence of the deposition morphologies was also studied optically in a symmetrical cell built with lithium electrodes. After passage of 28 mAh cm⁻², dendrite-free deposits were observed in a concentrated LiNO3 electrolyte. SEI characterization revealed that this LiNO3 concentrated electrolyte formed a Li₂O enriched and organic polymer depleted interphase.



Good: Low surface area with dense/globular morphology

KEYWORDS: anode-free battery, lithium metal anode, optical electrochemical cell, lithium nitrate, Li-ion battery, electrolyte, lithium dendrite

The use of metallic lithium anodes in rechargeable batteries has thus far been avoided due to dendritic growth during electrodeposition.^{1,2} These three-dimensional (3D) growths are often disconnected from the lithium surface, causing capacity fade, and can lead to dead lithium formation and electrolyte ignition from short circuiting.^{3,4} Because lithium is strongly reducing, the electrolyte decomposes on its surface to form a resistive solid electrolyte interphase (SEI), further consuming the lithium.⁵ If a dense, uniformly thick layer of lithium could be electrodeposited in the charging half-cycles, the formation of dead lithium would be avoided. To this end, many electrolytes with different salt and solvent compositions have been studied.6-11

In academic research, it is common practice to compensate for the irreversible lithium loss associated with dead lithium and SEI formation by introducing a large excess of lithium through the use of lithium metal foil anodes. 12 Lithium-plated copper anode cells, commonly referred to as "anode-free cells," offer an alternative in the study of lithium metal batteries (LMBs). In these cells, the cathode is the lithium source and the lithium anode is formed on the copper substrate during the first charge.¹³ These lithium-limited cells allow for a deep cycling of the anode in close stoichiometry to the cathode, which is a critical parameter for a true full cell, LMB. 14 In the absence of the lithium foil anode, the capacity decay is

dominated by the loss of the lithium source, not by an increase in cell resistance from an ionically insulating dead lithium layer. 12 Although some work has been done with anode-free cells, 15-17 there exists no comprehensive report on the capacity retention of lithium-limited cells in common electrolyte compositions. Morphologies of lithium deposits have been primarily investigated through scanning electron microscopy from electrodes cycled in coin cells. However, because lithium is ductile and deforms under mild stress, the morphology of the deposits is inevitably altered under the compressive forces induced by coin cells. Information regarding the extent of 3D growth and deposition thickness is therefore lost due to the compressive nature of the coin cell. 18 This problem can be circumvented by high-resolution, in situ optical imaging of the electrodes.3,4,11

In order to eliminate the effects of compressive forces and large excess of lithium on the cyclability of the lithium anode, optical imaging in conjunction with anode-free cells is utilized to study the true morphology and cyclability of lithium. Sampling a large variety of electrolytes, the lithium-limited cells reveal that the plating capacity is best retained in a 4 M lithium

Received: July 19, 2018 Accepted: October 15, 2018 Published: October 15, 2018



[†]McKetta Department of Chemical Engineering, The University of Texas at Austin, Austin, Texas 78712-1589, United States

[‡]Texas Materials Institute, The University of Texas at Austin, Austin, Texas 78712-1591, United States

[§]Department of Chemistry, The University of Texas at Austin, Austin, Texas 78712-1224, United States

Center for Electrochemistry, The University of Texas at Austin, Austin Texas 78712-0165, United States

[⊥]Shell International Exploration & Production Inc., Houston, Texas 77082, United States

ACS Applied Energy Materials

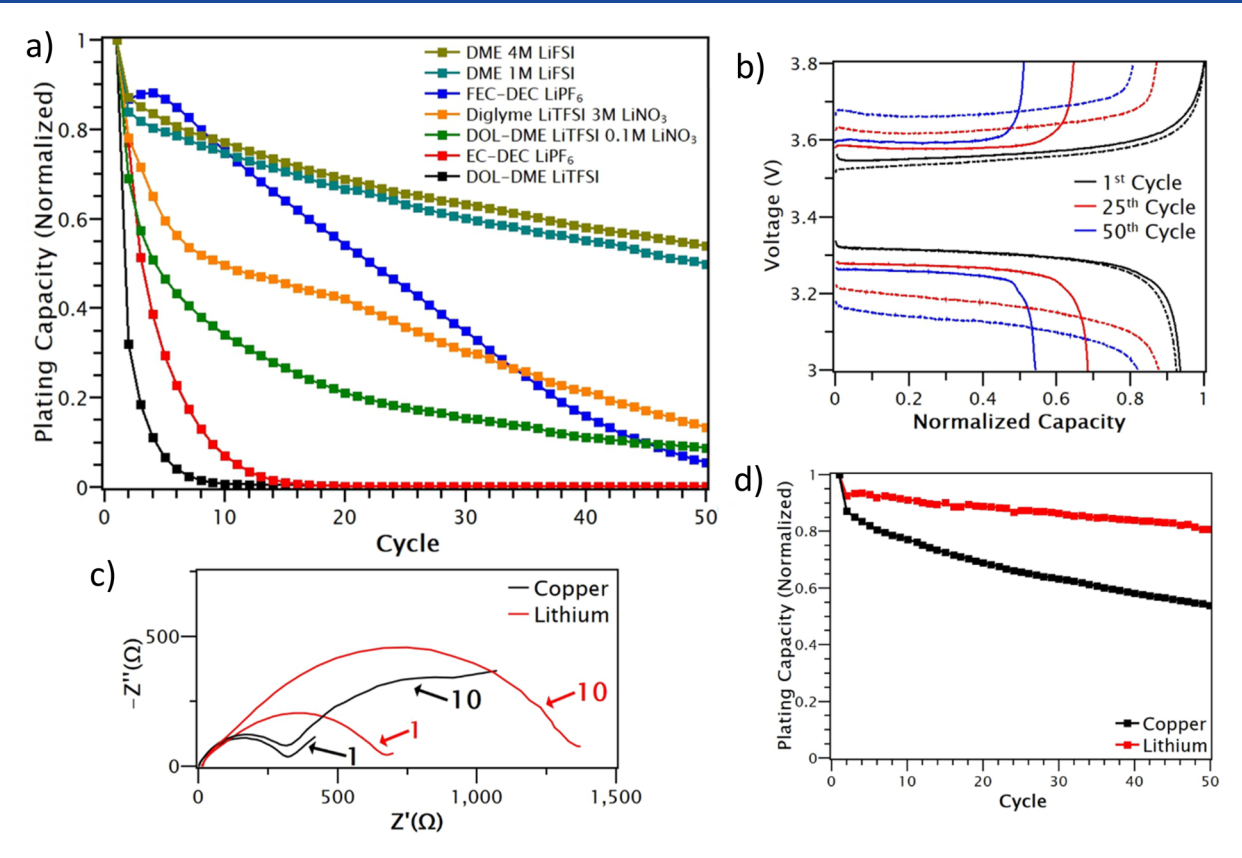


Figure 1. (a) Retention of the Coulombic capacity of LFPICu cells for different electrolytic solutions normalized to the first cycle. (b) Charge/discharge voltage profiles for the 1st, 25th, and 50th cycles of the 4 M LiFSI with DME in LFPICu (solid) and LFPILi (dashed) cells. (c) 1st and 10th cycle electrochemical impedance spectra of LFPICu and LFPILi cells for the 4 M LiFSI in DME from the cells cycled in panel d. (d) Comparison of the capacity retention of LFPICu and LFPILi cells.

bis(fluorosulfonyl)imide (LiFSI) in dimethoxyethane (DME) electrolyte after 50 cycles, although a 1 M LiPF₆ in fluoroethylene carbonate (FEC)/ethylene carbonate (EC) electrolyte demonstrated superior capacity retention in the early cycles. Though electrolyte formulations utilizing fluorinated ethylene carbonate (FEC)⁹ or high LiFSI salt concentrations⁷ have claimed to render compact and dendrite-free morphology, optical imaging of symmetrical lithium foil cell electrodes reveals that only lithium deposited from a concentrated LiNO₃ electrolyte is globular, rather than being dendritic, even after passage of 27.5 mAh cm⁻² of charge at 0.5 mA cm⁻². Through time-of-flight secondary ion mass spectrometry (ToF-SIMS) depth profiling, the nascent SEI formed on lithium foil in the concentrated LiNO₃ electrolyte is found to be rich in Li₂O with reduced organic polymer species.

Figure 1a shows the retention of the Coulombic capacity of the plated lithium normalized to the first cycle for different electrolytes in cells with copper and lithium iron phosphate (LFP) electrodes. All cells were cycled at 0.2 mA cm⁻² and had initial capacities of approximately 1.7 mAh cm⁻², which was in line with the theoretical capacity of their LFP electrodes. In the electrolytes with two solvents the v/v solvent ratio was 1:1. The capacity was best retained after 50 cycles with the 4 M LiFSI in DME electrolyte, consistent with earlier results from Zhang and co-workers. The superior performance of this electrolyte is attributed to the high-concentration salt reducing the number of free solvent molecules, lithium passivating LiF formation (from the fluorine present in the concentrated LiFSI), and minimal polymerization of the solvent DME. Decreasing the concentration of LiFSI in DME to 1 mol L⁻¹

resulted in similar capacity decay, although a lower initial Coulombic efficiency (ICE) was achieved. Given the high reactivity of the LiFSI salt and the stability of the DME solvent, 19,20 it appears the only value gained from increasing the salt concentration 4-fold is a few percent increase in the ICE. The rapid loss of capacity in the 1 M LiPF₆ in ethylene carbonate (EC)/diethyl carbonate (DEC) electrolytic solution is improved when the EC is replaced by singly fluorinated ethylene carbonate (FEC), in which lithium can extract the solvent fluorine to form a LiF enriched passivation layer. This FEC electrolyte provided the best capacity retention in the initial cycles but was less effective in the later cycles (Figure 1a). The addition of 0.1 M LiNO₃ to the 1 M lithium bis(trifuloromethylsulfonyl)amine (LiTFSI) in dioxolane (DOL)/DME improved capacity retention. This is attributed to the highly oxidizing nature of LiNO3 which forms a passivating Li₂O layer on the lithium surface. The 0.5 M LiTFSI with 3 M LiNO₃ in diethylene glycol dimethyl ether (diglyme) electrolyte introduced by Adams et al., had a higher capacity retention than the low-concentration LiNO3 electrolyte.

Capacity retention of an LFPlCu cell with 4 M LiFSI in DME was compared to a cell with a lithium foil anode (LFPl Li) in Figure 1d. As expected, the excess lithium compensates for the dead lithium retaining over 80% of the initial plating capacity after 50 cycles while the anode-free cell retains less than 60%. The residual capacity fade in the LFPlLi cells is attributed to the increased ionic resistance as the thickness of the dead lithium layer continuously increases.²² This can be seen in the greater voltage hysteresis of the LFPlLi cells when

ACS Applied Energy Materials

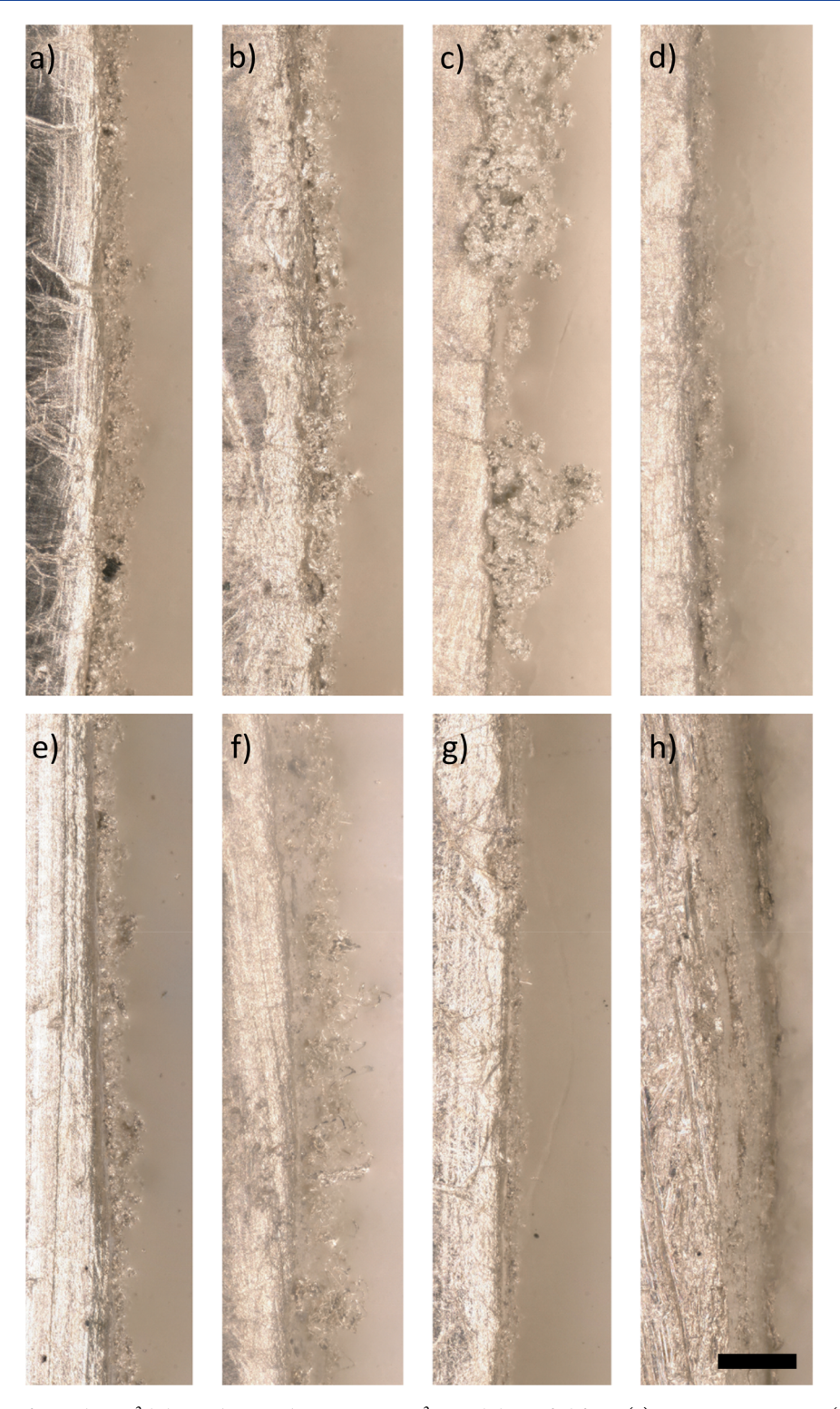


Figure 2. Morphologies of 3 mAh cm $^{-2}$ lithium deposited at 0.5 mA cm $^{-2}$ onto lithium foil from (a) 1 M LiFSI in DME, (b) 4 M LiFSI in DME, (c) 1 M LiTFSI in DOL/DME, (d) 1 M LiTFSI with 100 mM LiNO₃ in DOL/DME, (e) 1 M LiPF₆ in EC/DEC, (f) 1 M LiPF₆ in EC/DEC with 2% vinylene carboante, (g) 1 M LiPF₆ in FEC/DEC, and (h) 0.5 M LiTFSI with 3 M LiNO₃ in diglyme. The scale bar is 200 μ m.

compared to the LFPlCu cells (Figure 1b). Charge/discharge curves for the cycled LFPlCu (solid) and LFPlLi (dashed) cells utilizing 4 M LiFSI in DME shows that the voltage difference between the first and 50th cycles is less than 100 mV for the LFPlCu cells; this voltage difference is doubled when the copper substrate is replaced with the standard lithium foil electrode. The impedance spectra of the lithium and copper

cells in the discharged state also show a difference in their interphases (Figure 1c). The impedance spectra for the anodefree cells shows a smaller overall impedance with a depressed semicircle and tail in the low-frequency range. This is also seen in the impedance spectra of LFP|Cu cells with other electrolytes (Supporting Information Figure S1). On the other hand, the lithium foil anode cells' impedance spectra

ACS Applied Energy Materials

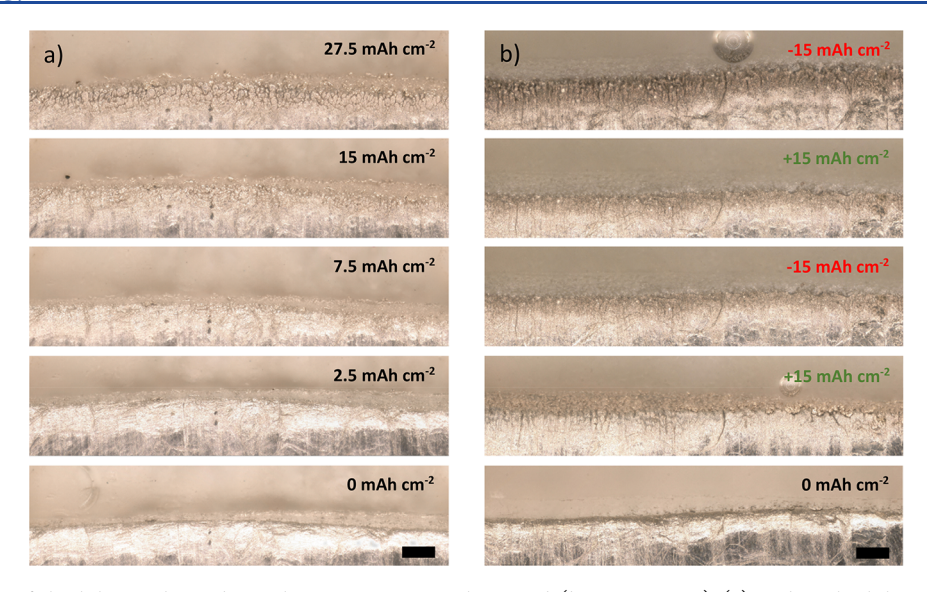


Figure 3. Morphology of the lithium electrode as charge is continuously passed (bottom to top) (a) and as the lithium electrode is charged/discharged (b) sequentially (from the bottom image to the top) with 3 M LiNO₃ and 0.5 M LiTFSI in diglyme. The scale bars are 200 μ m.

are dominated by a larger, depressed semicircle. On the 10th cycle, the tail end of the copper cell's impedance curve grows while maintaining a depressed semicircle in the high-frequency range with a similar diameter to the first cycle semicircle. The lithium cell impedance curve in the 10th cycle is still dominated by the depressed semicircle, only its diameter has roughly doubled in size. These differences in impedance spectra are caused by the difference in lithium surface conditions. Unlike the lithium foil that is passivated by a layer of oxide, nitride, or oxynitride of lithium, nascent lithium deposited on the copper current collector has no such oxide.² For this reason, the shape and overall impedance differences in the Nyquist plots in the first cycle are different (even though the impedance contribution from the dead lithium in the first cycle should be approximately equal in both the lithium and copper cells).2

Figure 2 shows high-resolution optical imaging of lithium depositions onto lithium substrates in various electrolytic solutions after 3 mAh cm⁻² of charge was passed at 0.5 mA cm⁻²; this quantity of charge was sufficient to observe dendritic growths. This electrochemical visualization cell was constructed with two lithium electrodes and no separator. The cell was flooded with electrolyte and hermetically sealed inside a glovebox. Pristine lithium electrodes, prior to deposition, are shown in Figure S2. The effect of current density on the deposit morphology is demonstrated in Figure S3; here, it is shown that the charge rate can alter deposition morphology. A schematic illustrating the optical cell design is shown in Figure S4.

As seen in Figure 2a,b, increasing the salt concentration of the LiFSI in DME, which substantially increased the electrolyte viscosity, did not affect the morphology of the deposit; 3D, foil-like depositions persisted. This indicates that the deposition morphologies were not dominated by concentration polarization or differences in SEI from the increased FSI-anion concentration. The addition of 0.1 M LiNO₃ (Figure 2d) to the 1 M LiTFSI in DOL/DME (Figure 2c) resulted in a reduction in deposition thickness, i.e., decreased porosity. The same effect was observed when the EC in the 1 M LiPF₆ in EC/DEC (Figure 2e) was replaced with FEC (Figure 2g) as reported by other groups. The addition of 2% (by volume)

vinylene carbonate to the 1 M LiPF $_6$ in EC/DEC increased the average dendrite heights in our visualization cell despite improvements in the Coulombic capacity retention observed in coin cell testing (Figure S5). This is likely due to the effect of the coin cell stack pressure on the lithium deposit as lithium cycling efficiency can be improved with increasing electrode compression (Figure S6). 10

Remarkably, at a high concentration of LiNO₃ (0.5 M LiTFSI with 3 M LiNO₃ in diglyme) no dendrites grew (Figure 2h); the deposit appeared dense with globular morphology. Figure 3a shows that this deposition morphology was retained even after 27.5 mAh cm⁻² of charge was passed at 0.5 mA cm⁻². It has already been reported previously that globular deposition morphology is induced when LiNO3 is present in the electrolyte.²⁶ However, these reports show that 3D electrodeposition evolves from the globular, nascent lithium as more charge is passed.²⁶ Additionally, SEM imaging of lithium depositions in 4 M LiFSI in DME and 3 M LiNO₃ with 0.5 M LiTFSI in diglyme shown in previous reports demonstrate similar morphology, but we find different deposition behavior utilizing optical imaging.^{6,7} This validates the use of a specialized visualization cell since morphology altering compressive forces no longer influence the lithium electrodeposits. Additionally, the globular and compact deposition behavior is retained even after charging/discharging large amounts of lithium at a faster rate of 1 mA cm⁻² (Figure

The absence of dendrites in the high-concentration LiNO₃ electrolyte was not associated with the best capacity retention (Figure 1a), though. The SEI formed in this electrolyte may be continuously growing a resistive Li₂O passivating layer on the deposit which diminishes the columbic efficiency.⁶ An "optimal" SEI should be capable of eliminating the formation of 3D structures, which ensures dangerous cell shorting will not occur and minimizes further SEI formation, and easily passivate the lithium surface so that a high cycling efficiency is achieved. In Figure 1a, it is shown that the cycling efficiency of lithium in the 4 M LiFSI compared to the 1 M LiPF₆ in EC/DEC is superior despite having similar deposition morphologies (Figure 2b,e). Thus, the ability of the electrolyte to passivate the lithium surface with minimal lithium loss may be

a larger contributor to improved cycling efficiency than the mitigation of 3D surfaces.²⁷ The observed morphology in the optical imaging of lithium electrodepositions should not be used as an indicator of improved cycling efficiency. This is true even in electrolytes where dendrite-free depositions occur despite the fact that less SEI should have to form on a smaller surface area.

Time-of-flight secondary ion mass spectrometry (ToF-SIMS) depth profiling of the SEI formed in different electrolytes is shown in Figure 4. For the ether electrolytes

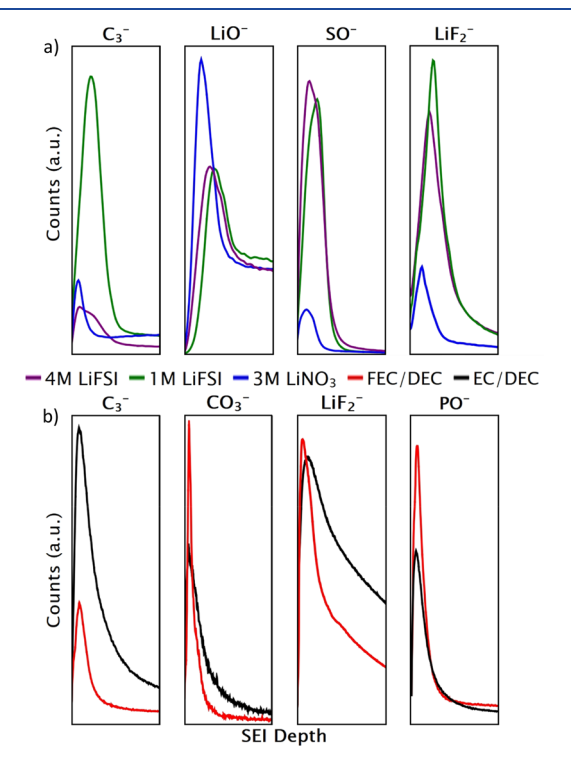


Figure 4. ToF-SIMS depth profile of lithium soaked in ether- (a) and carbonate-based (b) electrolytes for 12 h. All depth profiles have the same x-axis range with different y-axis ranges (for visual clarity).

(Figure 4a), the ionic species were chosen based on salt/ solvent decomposition products: C₃ was the proxy for organics such as lithium alkoxides or polyolefins; LiO- for the LiO₂ formed by LiNO₃; SO⁻ for the TFSI⁻ salt forming Li₂S_xO_y; and LiF₂⁻ formed from the fluorinated anions.^{6,19,20} For the carbonate electrolytes the ions were C_3^- for organics; CO₃⁻ for Li₂CO₃ and organic-carbonate species derived of FEC, DEC, and EC; LiF₂⁻ for the LiF formed from the PF₆⁻ and FEC; and PO from salt-reacted PF₆ forming Li_xPO_yF_z. 8,11,28

ToF-SIMS depth profiles show that the inorganic layer of the SEI, represented by the LiO-, SO-, and LiF2- curves, was largely unaffected by increasing the LiFSI concentration from 1 to 4 M (Figure 4a). Perhaps the limited reactivity of the solvent combined with the full decomposition of the salt ensures an inorganic rich SEI even with a 3 M concentration difference. 19,20 The C₃ curves show that the organic matter in the SEI is reduced with high LiFSI and LiNO3 salt concentrations. This could be due to the smaller amount of free solvent molecules present at higher salt concentrations. While passivating Li₂O forms to some extent in all the ether electrolytes, the high LiNO3 concentration induces a more pronounced Li₂O layer. As expected, fast Li⁺ conducting

nitrides (Li₃N) were absent since they are unable to passivate the lithium; LiN⁻ and Li₂N⁻ were not detected. The NO⁻ and NO₂ fragments from Li_xNO_y also showed no notable differences in a comparison of all the ether electrolytes. In carbonate electrolytes (Figure 4b), the organics in the SEI (C₃⁻) also decreased when FEC was present and an improved, thinner LiF film was formed. With the FEC, the SEI was also richer in Li₂CO₃ and contained more Li_xPO_yF_z product when compared to the unfluorinated EC electrolyte indicating an overall more inorganic rich SEI. Evidently, when the lithium is sufficiently passivated by a Li₂O or LiF enriched SEI, a thinner organic film is formed. Overall, the passivating Li₂O and LiF films can improve lithium capacity retention, LiF being the more desirable decomposition product for efficient lithium cyclability.

In conclusion, the use of anode-free cells allowed for a direct measure of lithium loss in lithium-limited cells. The 4 M LiFSI in DME electrolyte in the present study demonstrated the best capacity retention of all the electrolytes tested; however, the electrodeposited lithium from this electrolyte exhibited morphology similar to lithium deposited from other poor capacity retaining electrolytes. Optical imaging of electrodeposited lithium revealed that the high-concentration LiNO₃ electrolyte could inhibit dendrite formation even at high specific capacities. Finally, ToF-SIMS depth profiling was employed to probe the nascent SEI layer formed on lithium foil. It was found that high salt content reduced the amount of organic SEI layer present; high fluorine content also had a similar effect. Additionally, the role of the high-concentration LiNO₃ salt appeared to be the formation of a more Li₂O rich SEI. From the ToF-SIMS depth profiling, it appears possible that an SEI enriched with appropriate amounts of LiF and Li₂O could inhibit dendrite formation without the aid of compressive forces and provide high capacity retention. The results shown here suggest that the LFPICu cells are an effective means of studying the lithium metal anode, and the dendrite suppressing capabilities of the LiNO3 additive show great promise in LMBs.

ASSOCIATED CONTENT

S Supporting Information

The Supporting Information is available free of charge on the ACS Publications website at DOI: 10.1021/acsaem.8b01194.

Additional optical imaging (including pristine electrodes from Figure 2), impedance measurements, coin cell cycling, experimental details, equipment, and material information (PDF)

AUTHOR INFORMATION

Corresponding Author

*E-mail: mullins@che.utexas.edu.

Andrei Dolocan: 0000-0001-5653-0439 Adam Heller: 0000-0003-0181-1246 C. Buddie Mullins: 0000-0003-1030-4801

Notes

The authors declare no competing financial interest.

ACKNOWLEDGMENTS

We acknowledge the generous support provided by Shell and the Welch Foundation (via Grants F-1131 (A.H.) and F-1436 (C.B.M.)) as well as the National Science Foundation via Grant CBET-1603491. We also thank Celgard Corp. for their provision of separators and Solvay Fluor for their donation of fluoroethylene carbonate. We additionally thank Dr. Krishnaswamy Ravi-Chandar for use of his Keyence VHX-5000 digital microscope.

REFERENCES

- (1) Lin, D.; Liu, Y.; Cui, Y. Reviving the Lithium Metal Anode for High-Energy Batteries. *Nat. Nanotechnol.* **2017**, *12*, 194–206.
- (2) Cheng, X.-B.; Zhang, R.; Zhao, C.-Z.; Zhang, Q. Toward Safe Lithium Metal Anode in Rechargeable Batteries: A Review. *Chem. Rev.* **2017**, *117*, 10403—10473.
- (3) Rodriguez, R.; Loeffler, K. E.; Nathan, S. S.; Sheavly, J. K.; Dolocan, A.; Heller, A.; Mullins, C. B. In Situ Optical Imaging of Sodium Electrodeposition: Effects of Fluoroethylene Carbonate. *ACS Energy Lett.* **2017**, *2*, 2051–2057.
- (4) Wood, K. N.; Kazyak, E.; Chadwick, A. F.; Chen, K.-H.; Zhang, J.-G.; Thornton, K.; Dasgupta, N. P. Dendrites and Pits: Untangling the Complex Behavior of Lithium Metal Anodes through Operando Video Microscopy. ACS Cent. Sci. 2016, 2, 790–801.
- (5) Peled, E. The Electrochemical Behavior of Alkali and Alkaline Earth Metals in Nonaqueous Battery Systems—The Solid Electrolyte Interphase Model. *J. Electrochem. Soc.* 1979, 126, 2047–2051.
- (6) Adams, B. D.; Carino, E. V.; Connell, J. G.; Han, K. S.; Cao, R.; Chen, J.; Zheng, J.; Li, Q.; Mueller, K. T.; Henderson, W. A.; Zhang, J.-G. Long Term Stability of Li-S Batteries Using High Concentration Lithium Nitrate Electrolytes. *Nano Energy* **2017**, *40*, 607–617.
- (7) Qian, J.; Henderson, W. A.; Xu, W.; Bhattacharya, P.; Engelhard, M.; Borodin, O.; Zhang, J.-G. High Rate and Stable Cycling of Lithium Metal Anode. *Nat. Commun.* **2015**, *6*, 6362.
- (8) Zhang, X.-Q.; Cheng, X.-B.; Chen, X.; Yan, C.; Zhang, Q. Fluoroethylene Carbonate Additives to Render Uniform Li Deposits in Lithium Metal Batteries. *Adv. Funct. Mater.* **2017**, *27*, 1605989.
- (9) Markevich, E.; Salitra, G.; Chesneau, F.; Schmidt, M.; Aurbach, D. Very Stable Lithium-Metal Stripping/Plating at a High Rate and High Areal Capacity in Fluoroethylene Carbonate-Based Organic Electrolyte Solution. *ACS Energy Lett.* **2017**, *2*, 1321–1326.
- (10) Ota, H.; Shima, K.; Ue, M.; Yamaki, J. Effect of Vinylene Carbonate as Additive to Electrolyte for Lithium Metal Anode. *Electrochim. Acta* **2004**, *49*, 565–572.
- (11) Wood, S. M.; Pham, C. H.; Rodriguez, R.; Nathan, S. S.; Dolocan, A. D.; Celio, H.; de Souza, J. P.; Klavetter, K. C.; Heller, A.; Mullins, C. B. K+ Reduces Lithium Dendrite Growth by Forming a Thin, Less-Resistive Solid Electrolyte Interphase. *ACS Energy Lett.* **2016**, *1*, 414–419.
- (12) Albertus, P.; Babinec, S.; Litzelman, S.; Newman, A. Status and Challenges in Enabling the Lithium Metal Electrode for High-Energy and Low-Cost Rechargeable Batteries. *Nat. Energy* **2018**, *3*, 16–21.
- (13) Neudecker, B. J.; Dudney, N. J.; Bates, J. B. Lithium-Free" Thin-Film Battery with In Situ Plated Li Anode. *J. Electrochem. Soc.* **2000**, *147*, 517–523.
- (14) Shi, Q.; Zhong, Y.; Wu, M.; Wang, H.; Wang, H. High-Capacity Rechargeable Batteries Based on Deeply Cyclable Lithium Metal Anodes. *Proc. Natl. Acad. Sci. U. S. A.* **2018**, *115*, 5676–5680.
- (15) Zhang, S. S.; Fan, X.; Wang, C. A Tin-Plated Copper Substrate for Efficient Cycling of Lithium Metal in an Anode-Free Rechargeable Lithium Battery. *Electrochim. Acta* **2017**, 258, 1201–1207.
- (16) Qian, J.; Adams, B. D.; Zheng, J.; Xu, W.; Henderson, W. A.; Wang, J.; Bowden, M. E.; Xu, S.; Hu, J.; Zhang, J.-G. Anode-Free Rechargeable Lithium Metal Batteries. *Adv. Funct. Mater.* **2016**, *26*, 7094–7102.
- (17) Assegie, A. A.; Cheng, J.-H.; Kuo, L.-M.; Su, W.-N.; Hwang, B.-J. Polyethylene Oxide Film Coating Enhances Lithium Cycling Efficiency of an Anode-Free Lithium-Metal Battery. *Nanoscale* **2018**, 10, 6125–6138.
- (18) Harrison, K. L.; Zavadil, K. R.; Hahn, N. T.; Meng, X.; Elam, J. W.; Leenheer, A.; Zhang, J.-G.; Jungjohann, K. L. Lithium Self-

- Discharge and Its Prevention: Direct Visualization through *In Situ* Electrochemical Scanning Transmission Electron Microscopy. *ACS Nano* **2017**, *11*, 11194–11205.
- (19) Eshetu, G. G.; Diemant, T.; Grugeon, S.; Behm, R. J.; Laruelle, S.; Armand, M.; Passerini, S. In-Depth Interfacial Chemistry and Reactivity Focused Investigation of Lithium—Imide- and Lithium—Imidazole-Based Electrolytes. ACS Appl. Mater. Interfaces 2016, 8, 16087—16100.
- (20) Camacho-Forero, L. E.; Smith, T. W.; Balbuena, P. B. Effects of High and Low Salt Concentration in Electrolytes at Lithium-Metal Anode Surfaces. *J. Phys. Chem. C* **2017**, *121*, 182–194.
- (21) Park, M. S.; Ma, S. B.; Lee, D. J.; Im, D.; Doo, S.-G.; Yamamoto, O. A Highly Reversible Lithium Metal Anode. *Sci. Rep.* **2015**, *4*, 3815.
- (22) Lu, D.; Shao, Y.; Lozano, T.; Bennett, W. D.; Graff, G. L.; Polzin, B.; Zhang, J.; Engelhard, M. H.; Saenz, N. T.; Henderson, W. A.; Bhattacharya, P.; Liu, J.; Xiao, J. Failure Mechanism for Fast-Charged Lithium Metal Batteries with Liquid Electrolytes. *Adv. Energy Mater.* 2015, *5*, 1400993.
- (23) Gireaud, L.; Grugeon, S.; Laruelle, S.; Yrieix, B.; Tarascon, J.-M. Lithium Metal Stripping/Plating Mechanisms Studies: A Metallurgical Approach. *Electrochem. Commun.* **2006**, *8*, 1639–1649.
- (24) Aurbach, D. Review of Selected Electrode-Solution Interactions Which Determine the Performance of Li and Li Ion Batteries. *J. Power Sources* **2000**, *89*, 206–218.
- (25) Bai, P.; Li, J.; Brushett, F. R.; Bazant, M. Z. Transition of Lithium Growth Mechanisms in Liquid Electrolytes. *Energy Environ. Sci.* **2016**, *9*, 3221–3229.
- (26) Li, W.; Yao, H.; Yan, K.; Zheng, G.; Liang, Z.; Chiang, Y.-M.; Cui, Y. The Synergetic Effect of Lithium Polysulfide and Lithium Nitrate to Prevent Lithium Dendrite Growth. *Nat. Commun.* **2015**, *6*, 7436.
- (27) Ding, F.; Xu, W.; Graff, G. L.; Zhang, J.; Sushko, M. L.; Chen, X.; Shao, Y.; Engelhard, M. H.; Nie, Z.; Xiao, J.; Liu, X.; Sushko, P. V.; Liu, J.; Zhang, J.-G. Dendrite-Free Lithium Deposition via Self-Healing Electrostatic Shield Mechanism. *J. Am. Chem. Soc.* **2013**, *135*, 4450–4456.
- (28) Leung, K.; Soto, F.; Hankins, K.; Balbuena, P. B.; Harrison, K. L. Stability of Solid Electrolyte Interphase Components on Lithium Metal and Reactive Anode Material Surfaces. *J. Phys. Chem. C* **2016**, 120, 6302–6313.